



Analytical diagonal elements of regularized meshless method for regular domains of 2D Dirichlet Laplace problems

Wen Chen^{a,*}, Rencheng Song^b

^a Department of Engineering Mechanics, Hohai University, Nanjing, Jiangsu, China

^b Department of Mathematics, Zhejiang University, Hangzhou, Zhejiang, China

ARTICLE INFO

Article history:

Received 11 January 2009

Accepted 27 July 2009

Available online 19 August 2009

Keywords:

Regularized meshless method

Regular domain

Desingularization technique

Null fields equation

Analytical diagonal elements

ABSTRACT

This note is to present a simple approach to derive the analytical formula of the diagonal elements of the interpolation matrix of the regularized meshless method (RMM) for regular domain problems, which is a very new boundary-type numerical discretization technique. In literature, these diagonal elements are mostly calculated numerically by the desingular technique, except for the circular domain problems. Our numerical experiments show that the analytical diagonal elements can improve the solution accuracy of the RMM for some regular domain problems, and the diagonal elements are critical to the solution accuracy of the RMM. Thus, a searching process is employed to find the optimal diagonal elements for RMM.

© 2009 Elsevier Ltd. All rights reserved.

1. Introduction

In recent decades, meshless methods [1–6] have attracted a growing attention from mathematics and engineering communities. Generally speaking, these methods can be divided into the domain-type or boundary-type techniques, depending on if their basis functions satisfy the governing equation of interest. The regularized meshless method is one kind of the boundary type meshless collocation methods, proposed very recently by Young et al. (RMM) [7], as an alternative approach of the well-known method of fundamental solutions (MFS) [8,9]. The fictitious boundary and severely ill-conditioning interpolation matrix of the MFS are avoided in the RMM via the desingularization technique of subtracting and adding-back. Numerical results show that the RMM is very efficient in the solution of Laplace problems [7,10–12], the exterior acoustics problem [13], the acoustic eigenproblem [14], and the antiplane shear problem [15].

Because the interpolation basis functions of the RMM encounter singularity, the finite diagonal elements of its interpolation matrix have to be numerically calculated, except for the circular domain case [7]. In this study, we derive the analytical diagonal elements of the RMM for the other regular domains problems, such as polygonal domain, etc. The accuracy of RMM solution using such analytical diagonal elements is found improved in some examples than that using the traditional numerical diagonal elements. It also shows that the RMM solution accuracy is closely related to the accuracy of diagonal elements.

A searching process is then proposed to improve the accuracy of RMM solution further.

2. Regularized meshless method

We consider Laplace equation with the Dirichlet boundary conditions

$$\nabla^2 u(x, y) = 0 \quad \text{in } D, \quad (1)$$

$$u(x, y) = f \quad \text{on } \Gamma, \quad (2)$$

where f is a known function, D the arbitrary domain, and $\Gamma = \partial D$ the boundary.

The solution of Eqs. (1) and (2) at $t = (x, y)$ is approximated in the RMM by

$$u(t) = \sum_{j=1}^N \alpha_j A(t, s_j), \quad t \in D, \quad (3)$$

where $A(t, s_j)$ is the chosen basis function, s_j represents the j th source node, and $\{\alpha_j\}_{j=1}^N$ denote the unknown coefficients. Note that the basis functions of the RMM satisfy the governing equation.

Eq. (3) is forced to satisfy the boundary condition (2) on N points $\{t_i\}_{i=1}^N$ on Γ . Then $\{\alpha_j\}_{j=1}^N$ can be solved from the resulting linear system.

In the RMM, $A(t_i, s_j)$ is the so-called double layer potential, namely,

$$A(t_i, s_j) = \frac{\langle (t_i - s_j), n_j \rangle}{r_{ij}^2},$$

* Corresponding author.

E-mail address: chenwen@hhu.edu.cn (W. Chen).

where $r_{ij} = |s_j - t_i|$, the symbol \langle, \rangle denotes the inner product of vectors, and n_j is the outward normal vector of interior problem at s_j . Notice that the sign of $A(t_i, s_j)$ here maybe opposite to some known results [12]. But it does not affect the solution accuracy of RMM. So it keeps the above form hereafter.

$A(t_i, s_j)$ is singular at origin when t_i approaches to s_j . And the RMM employs the desingularization technique of subtracting and adding-back to derive the finite diagonal elements. The reduced null-fields equation [7,16]

$$\int_{\Gamma} A^{(e)}(t_i, s) d\Gamma(s) = 0, \quad t_i \in D^e \quad (4)$$

is directly discretized by

$$\sum_{j=1}^N A^{(e)}(t_i, s_j) |l_j| = 0 \quad (5)$$

in the original RMM formulation, where $A^{(e)}$ is related to A by the opposite normal direction, $|l_j|$ is the half distance of the source nodes s_{j-1} and s_{j+1} , and D^e represents the exterior domain of D .

This note employs Eq. (4) to derive analytical diagonal elements without the direct discretization. The details are shown in Section 3.

3. Analytical diagonal elements

The line integral in Eq. (4) is divided into

$$\int_{\Gamma} A^{(e)}(t_i, s) d\Gamma(s) = \int_{l_i} A^{(e)}(t_i, s) d\Gamma(s) + \int_{\Gamma \setminus l_i} A^{(e)}(t_i, s) d\Gamma(s) = 0, \quad (6)$$

see Fig. 1, where s_i is the i th source node, l_i the short curve between $s_{i-1/2}$ and $s_{i+1/2}$, and $\Gamma \setminus l_i$ the long complementary curve of l_i .

Since the length of l_i is small (when N is large), the singular integral in Eq. (6) is approximated by

$$\int_{l_i} A^{(e)}(t_i, s) d\Gamma(s) \approx A^{(e)}(t_i, s_i) |l_i|. \quad (7)$$

From Eqs. (6) and (7), we get

$$A^{(e)}(t_i, s_i) = -\frac{1}{|l_i|} \int_{\Gamma \setminus l_i} A^{(e)}(t_i, s) d\Gamma(s). \quad (8)$$

Then

$$A(t_i, s_i) = A^{(e)}(t_i, s_i) = \frac{1}{|l_i|} \int_{\Gamma \setminus l_i} A(t_i, s) d\Gamma(s). \quad (9)$$

The relationships of kernel functions for interior and exterior problems are used in the above formula, namely,

$$A(t_i, s) = -A^{(e)}(t_i, s), \quad t_i \neq s,$$

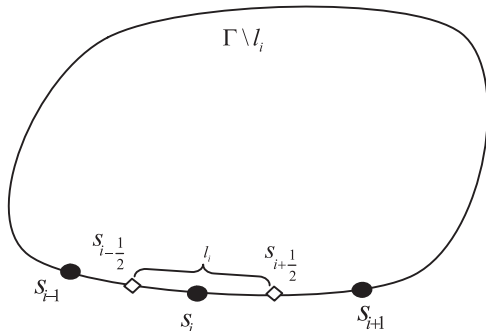


Fig. 1. The sketch of integration.

$$A(t_i, s_i) = A^{(e)}(t_i, s_i), \quad t_i = s_i,$$

see Ref. [7]. Eq. (9) can also be derived by the technique of subtracting and adding-back. This note calls the RMM with Eq. (9) as the analytical RMM. It is different from the RMM in Ref. [18], which is called the numerical RMM in this study with the diagonal elements

$$A(t_i, s_i) = A^{(e)}(t_i, s_i) = \frac{1}{|l_i|} \sum_{j \neq i}^N A(t_i, s_j) |l_j|. \quad (10)$$

It can be seen Eq. (10) is obtained by discretizing the integration in Eq. (9).

To be concise, $A(t_i, s_j)$ is denoted as $A(i, j)$ hereafter. The integrand $A^{(e)}(t_i, s)$ is non-singular on the curve $\Gamma \setminus l_i$. In some special cases, such as the circular or polygonal domains, $A(i, i)$ can be solved analytically from Eq. (9). We list two cases as follows.

Case 1: The circular domain. To consider the circular domain, we force the nodes $\{(x_i, y_i)\}_{i=1}^N$ on Γ to satisfy

$$x_i = R \cos(\theta_i), \quad y_i = R \sin(\theta_i), \quad (11)$$

where R is the radius of the circle, N the number of nodes, and $\theta_i = \pi/N + 2\pi/N(i-1)$ for $i = 1, 2, \dots, N$.

It is easy to get the diagonal elements from Eq. (9),

$$A(i, i) = -\frac{N}{2R} + \frac{1}{2R}, \quad i = 1, 2, \dots, N. \quad (12)$$

It is found that $A(i, i)$ in Eqs. (9) and (10) are equal on circular domains, since the integrand is constant in this case.

As known, the analytical diagonal elements given in Ref. [7] are

$$A(i, i) = -\frac{N}{2R} - \frac{1}{2R}, \quad i = 1, 2, \dots, N. \quad (13)$$

Numerical comparison will be done to show the accuracy of the two different diagonal elements for circular domain problems.

Case 2: The square domain. For the square domain, let the nodes $\{(x_j, y_j)\}_{j=1}^N$ on its four boundaries satisfy

$$(x_i, y_i) = \left(\frac{i}{K} - \frac{1}{2K}, 0 \right), \quad i = 1, 2, \dots, K,$$

$$(x_i, y_i) = \left(1, \frac{i-K}{K} - \frac{1}{2K} \right), \quad i = K+1, K+2, \dots, 2K,$$

$$(x_i, y_i) = \left(1 - \frac{i-2K}{K} + \frac{1}{2K}, 1 \right), \quad i = 2K+1, 2K+2, \dots, 3K,$$

$$(x_i, y_i) = \left(0, 1 - \frac{i-3K}{K} + \frac{1}{2K} \right), \quad i = 3K+1, 3K+2, \dots, N,$$

where K is the number of nodes on each boundary and $N = 4K$.

Then, by using Eq. (9), we obtain the analytical diagonal elements:

$$A(i, i) = K \left[\arctan\left(\frac{1}{x_i - 1}\right) + \arctan(-1 + x_i) - \arctan(x_i) - \arctan\left(\frac{1}{x_i}\right) \right]$$

for $i = 1, 2, \dots, K$;

$$A(i, i) = K \left[\arctan\left(\frac{1}{y_i - 1}\right) + \arctan(y_i - 1) - \arctan(y_i) - \arctan\left(\frac{1}{y_i}\right) \right]$$

for $i = K+1, K+2, \dots, 2K$;

$$A(i, i) = K \left[-\arctan\left(\frac{1}{x_i}\right) + \arctan(-1 + x_i) - \arctan(x_i) + \arctan\left(\frac{1}{x_i - 1}\right) \right]$$

for $i = 2K+1, 2K+2, \dots, 3K$;

$$A(i, i) = K \left[-\arctan\left(\frac{1}{y_i}\right) + \arctan(y_i - 1) - \arctan(y_i) + \arctan\left(\frac{1}{y_i - 1}\right) \right]$$

for $i = 3K+1, 3K+2, \dots, N$.

It is noted that the above derivation of the analytical diagonal elements, unfortunately, is not feasible for the Neumann boundary problem. We know

$$B(t_i, s_j) = \frac{\partial A(t_i, s_j)}{\partial \bar{n}_i} = 2 \frac{\langle (t_i - s_j), n_j \rangle \langle (t_i - s_j), \bar{n}_i \rangle}{r_{ij}^4} - \frac{\langle n_j, \bar{n}_i \rangle}{r_{ij}^2},$$

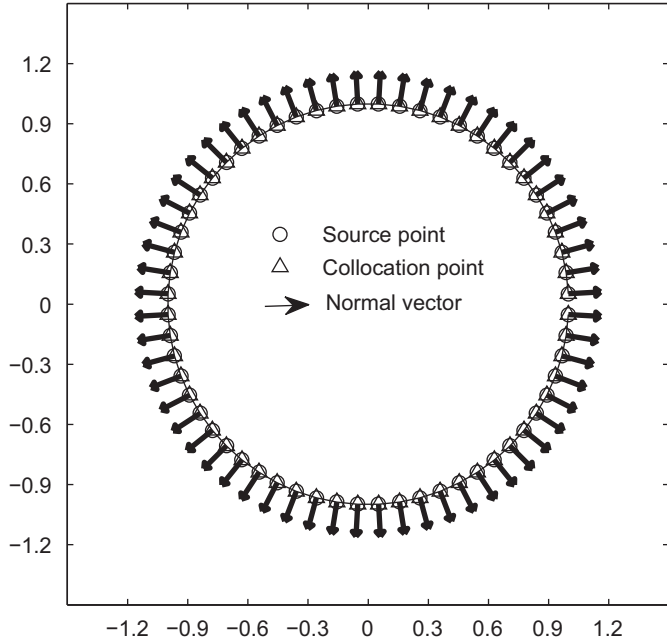


Fig. 2. Node distribution for circular domain ($N = 60$).

where $B(t_i, s_j)$ is the interpolation basis function used on Neumann boundary and \bar{n}_i is the outward normal vector at t_i . $B(t_i, s_j)$ has higher degree of singularity compared with $A(i, j)$. If we derive $B(t_i, s_i)$ in the same fashion, the analytical diagonal elements for the Neumann boundary should be

$$B(t_i, s_i) = B^{(e)}(t_i, s_i) = -\frac{1}{|l_i|} \int_{\Gamma_{l_i}} B(t_i, s) d\Gamma(s). \tag{14}$$

The diagonal element $B(t_i, s_i)$ in Eq. (14) is usually too large. This is because the integration $B(t_i, s)$ in Eq. (14) is nearly singular at the two ends of l_i . The exact value of $\int_{\Gamma_{l_i}} B(t_i, s) d\Gamma(s)$ is much larger than its discrete form $\sum_{j \neq i}^N B(t_i, s_j) |l_j|$, which makes the inference impossible.

4. Numerical results and discussions

In this section, three Dirichlet boundary problems are examined. The first problem is in the circular domain, the second in the square domain, and the third in the elliptic domain. To verify the validity of the analytical diagonal elements, the results of the present analytical diagonal RMM are compared with the numerical RMM in Ref. [18].

The error at point (x_i, y_j) is defined as

$$E_{ij} = |u(x_i, y_j) - \hat{u}(x_i, y_j)|^2, \tag{15}$$

where u and \hat{u} are the analytical and numerical solutions, respectively. The total average error on the whole domain is defined as

$$TE = \frac{1}{PQ} \sum_{i=1}^Q \sum_{j=1}^P E_{ij}, \tag{16}$$

where P and Q are the numbers of y_j and x_i in the domain.

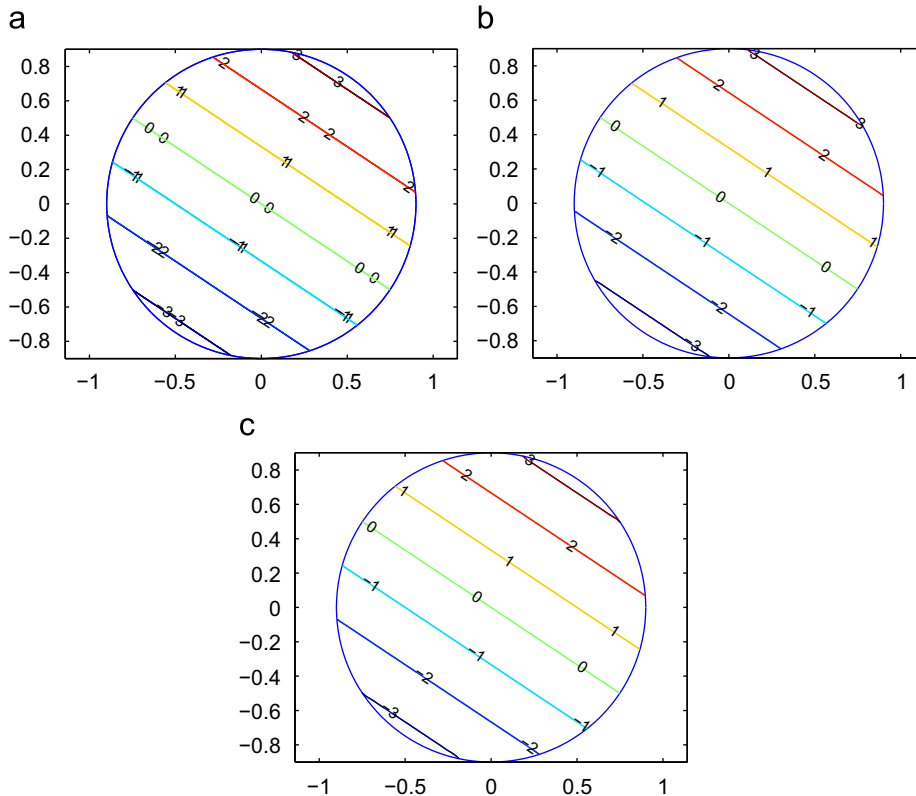


Fig. 3. The solution contours of Example 1 ($N = 60$): (a) exact solution, (b) solution of RMM with Eq. (12), and (c) solution of RMM with Eq. (13).

4.1. Example 1: The circular domain

The radius of the circular domain is $R = 1$. The exact solution of Example 1 is $u(x, y) = 2x + 3y$ subjected to the Dirichlet boundary condition

$$u = 2\cos(\phi) + 3\sin(\phi).$$

The problem sketch and node distribution are shown in Fig. 2.

To see the accuracy of different diagonal elements in Eqs. (12) and (13), the contours of RMM solutions are shown in Fig. 3. The solution of RMM with Eq. (13) is more accurate than that of our paper in Eq. (12). To clearly see this, the convergence curves of RMM are shown in Fig. 4, from which it can be seen the solutions of RMM with Eq. (13) converge more quickly than that of RMM with Eq. (12). It indicates the accuracy of diagonal element is critical to the solution accuracy of RMM. For the circular domain problem, the diagonal element in Eq. (12) (which also equals to Eq. (10) of the numerical RMM) is not optimal. The diagonal element in Eq. (13) is more accurate.

We further show that the diagonal elements in Eq. (13) is nearly optimal by searching the diagonal elements with a

perturbation. Namely, let $\tilde{A}(i, i) = \tilde{A}(i, i) + \delta$ be the new diagonal element, where $A(i, i)$ is the diagonal element in Eq. (12) and δ is a perturbation factor varying in the interval $[-2, 0]$ with a step 0.02. Note that δ is constant for different $A(i, i)$. The searching of a truly optimal diagonal element by $\tilde{A}(i, i) = A(i, i) + \delta(i)$ is a hard work, and will not be discussed here. The error curve is shown in Fig. 5. The minimal TE error in Eq. (16) is achieved at $\delta = -1.0$ with $TE = 1.822 \times 10^{-6}$. Similar error curves are also drawn (omitted here for saving space) with different radius R . It is found that the minimal error is always achieved when $\delta = -1/R$. Thus,

$$\tilde{A}(i, i) = -\frac{N}{2R} + \frac{1}{2R} + \left(-\frac{1}{R}\right) = -\frac{N}{2R} - \frac{1}{2R},$$

which is just the diagonal element $A(i, i)$ in Eq. (13).

4.2. Example 2: The square domain

The square domain problem is taken from [7]. Its exact solution is $u(x, y) = \sum_{j=1}^{\infty} C_n \sinh(n\pi(1-y)) \sin(n\pi x)$, where $C_n = 2(-1)^{n+1} / (n\pi) \sinh(n\pi)$. The Dirichlet boundary conditions are

$$u(x, 0) = x, \quad u(x, 1) = u(0, y) = u(1, y) = 0. \tag{17}$$

The problem sketch and the node distribution are shown in Fig. 6.

The RMM solution contours are plotted in Fig. 7. We can see the analytical and numerical RMM solutions are both quite close to the exact ones. This is not surprising because the diagonal elements of the two methods are almost the same except for those of the nodes near the four right angles. The convergence curves of the two methods are shown in Fig. 8. The errors of the two methods decrease quickly with N , while the rate of the analytical method is a little faster.

The numerical results show that the analytical diagonal element in Eq. (9) is effective for the square domain problem. Its solution accuracy is improved when the number of source nodes increases. It is stressed that similar behaviors have also been observed in other polygonal domains.

Finally, we also search the diagonal element by $\tilde{A}(i, i) = A(i, i) + \delta$, where $A(i, i)$ is the analytical diagonal element for square domain in our paper, and δ is a perturbation factor varies in the interval $[-0.5, 0.5]$ with the step 0.04. The error curve is shown in Fig. 9. The minimal error is $TE = 7.973 \times 10^{-8}$ achieved when $\delta = -0.05$. For comparison, we show that $TE = 1.030 \times 10^{-7}$ when $\delta = 0$, i.e., $\tilde{A}(i, i) = A(i, i)$. The improvement of the solution

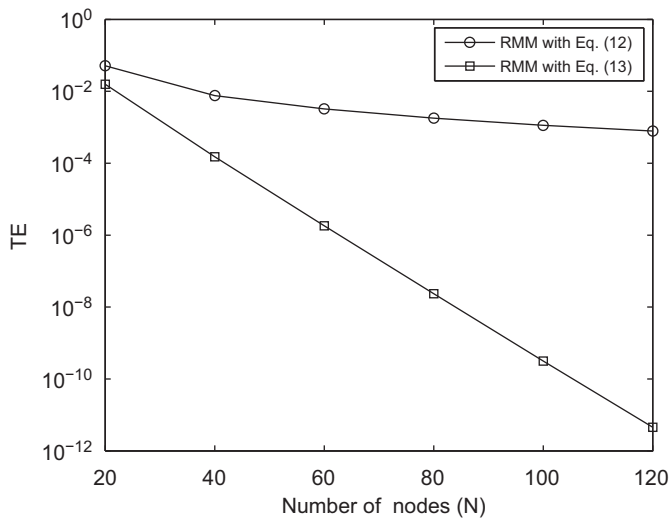


Fig. 4. The convergence curves of Example 1.

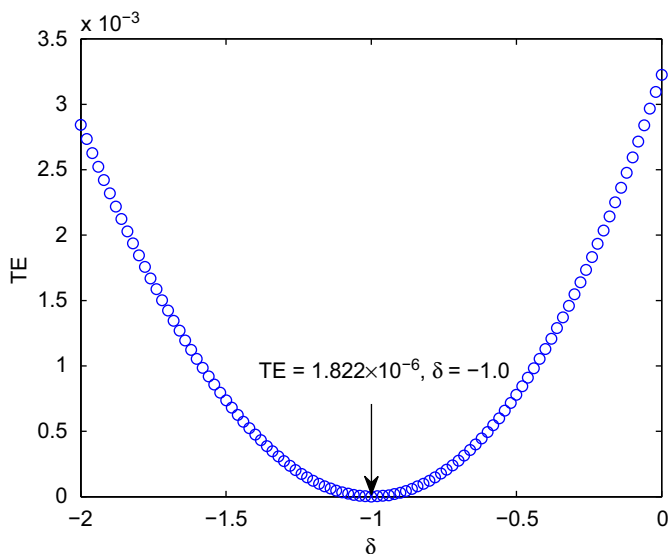


Fig. 5. The error curve of Example 1 with diagonal element $\tilde{A}(i, i)$ ($N = 60$).

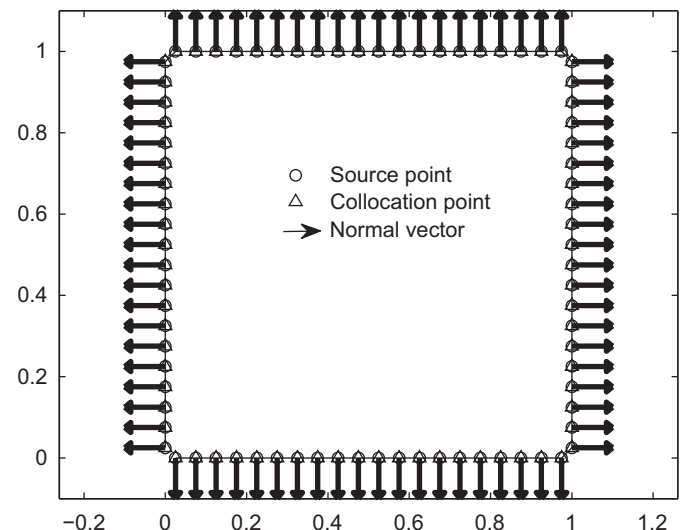


Fig. 6. Node distribution for square domain ($N = 80$).

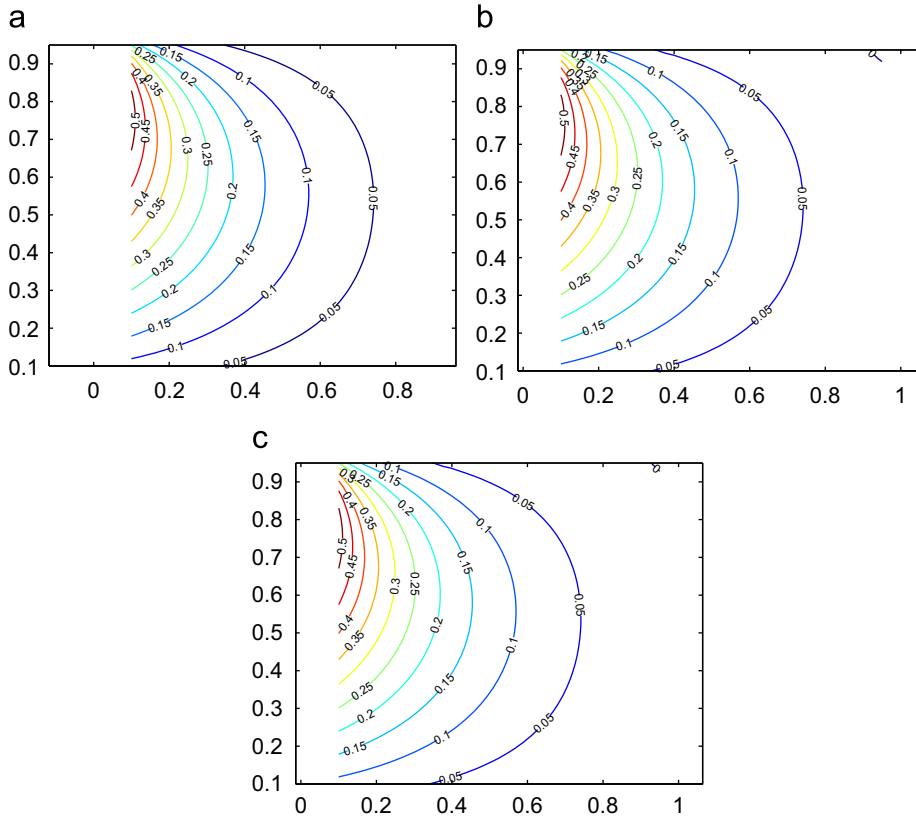


Fig. 7. The solution contours of Example 2 ($N = 80$): (a) exact solution, (b) numerical RMM, and (c) analytical RMM.

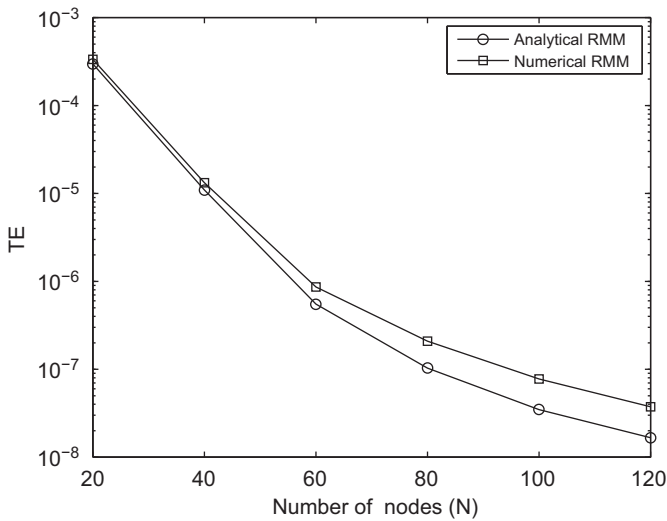


Fig. 8. The convergence curves of Example 2.

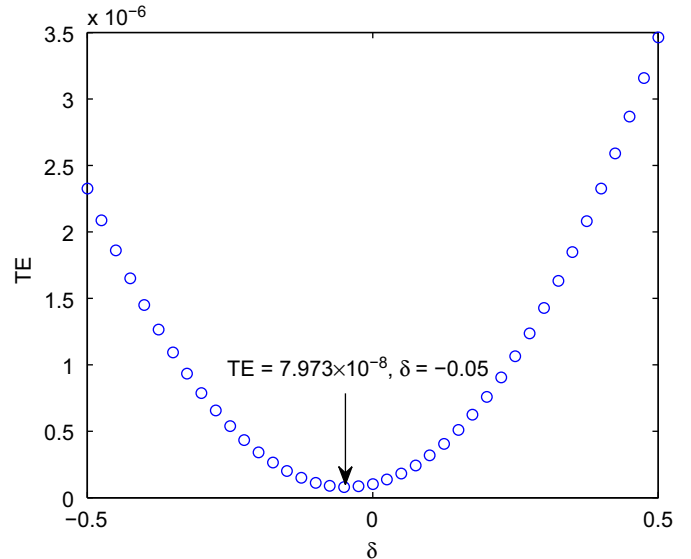


Fig. 9. The error curve of Example 2 with diagonal element $\hat{A}(i, i)$ ($N = 80$).

accuracy by searching diagonal elements is not obvious for the square domain problem.

4.3. Example 3: The elliptic domain

A Dirichlet elliptic domain problem is also considered. We notice that the diagonal element in Eq. (9) cannot be integrated analytically here. Thus, the “analytical” diagonal elements are obtained by the numerical integration, i.e., the adaptive Newton–Cotes 8-panel rule [17]. The main purpose of this case is to

show the validity and accuracy of our analytical method in arbitrary domains.

The major and minor semi axes of the elliptic domain are $R_1 = 1.0$ and $R_2 = 0.5$, respectively. The exact solution of Example 3 is $u(x, y) = x + y$ subjected to the boundary condition

$$u = R_1 \cos(\theta) + R_2 \sin(\theta).$$

The node distribution of the two methods is shown in Fig. 10.

Notice that, for this example, $S_{i-\frac{1}{2}}$ and $S_{i+\frac{1}{2}}$ in Fig. 1 are not midpoints of curves $S_{i-1}S_i$ and S_iS_{i+1} . Actually, they are defined as

$$S_{i-\frac{1}{2}} = (R_1 \cos(\theta_i - \frac{\pi}{N}), R_2 \sin(\theta_i - \frac{\pi}{N}))$$

$$S_{i+\frac{1}{2}} = (R_1 \cos(\theta_i + \frac{\pi}{N}), R_2 \sin(\theta_i + \frac{\pi}{N}))$$

here, where $\theta_i = \frac{\pi}{N} + (i - 1)\frac{2\pi}{N}$, $s_i = (R_1 \cos(\theta_i), R_2 \sin(\theta_i))$, and N is the total number of nodes.

The solution contours are drawn in Fig. 11, while the convergence curves are shown in Fig. 12. In the two figures, the

solution difference of the two methods is almost invisible. These results indicate the diagonal element in Eq. (9) is also effective for arbitrary domain problems. But the solution accuracy does not improve by the analytical RMM for the elliptic case.

Finally, we also search the diagonal element by $\tilde{A}(i, i) = A(i, i) + \delta$, where $A(i, i)$ is the analytical diagonal element in Eq. (9) (obtained by numerical integration for this example), and δ is a perturbation factor varying in the interval $[-5.0, 2.0]$ with a step 0.07. The error curve is shown in Fig. 13. The minimal error is $TE = 1.509 \times 10^{-4}$ achieved when $\delta = -1.22$. For comparison, it is shown that $TE = 4.449 \times 10^{-4}$ when $\delta = 0$, i.e., $\tilde{A}(i, i) = A(i, i)$. It indicates the accuracy of RMM solution

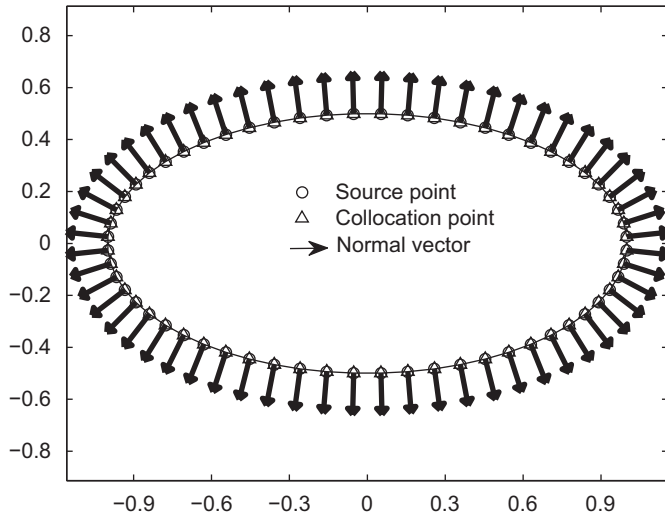


Fig. 10. Node distribution of elliptic domain ($N = 60$).

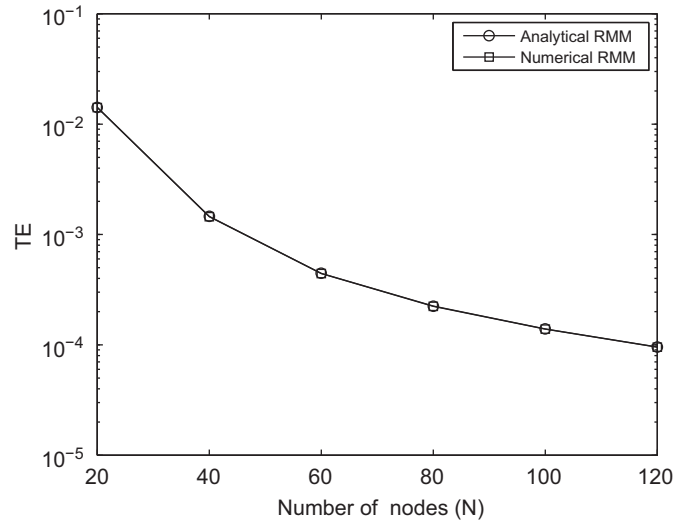


Fig. 12. The convergence curves of Example 3.

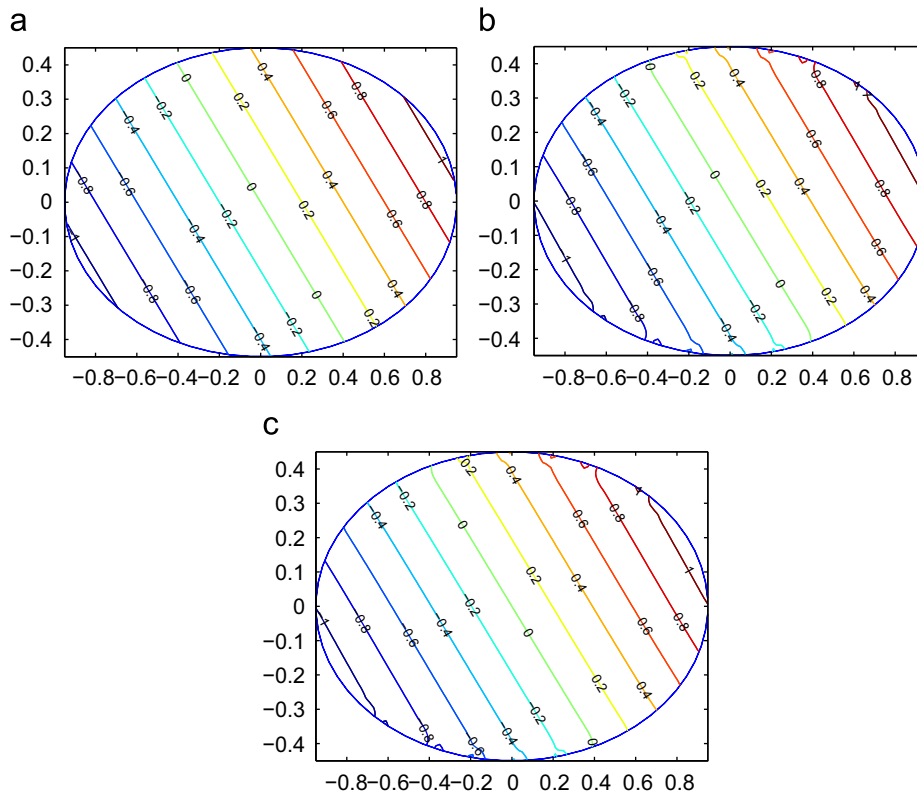


Fig. 11. The solution contours of Example 3 ($N = 60$): (a) exact solution, (b) numerical RMM, and (c) analytical RMM.

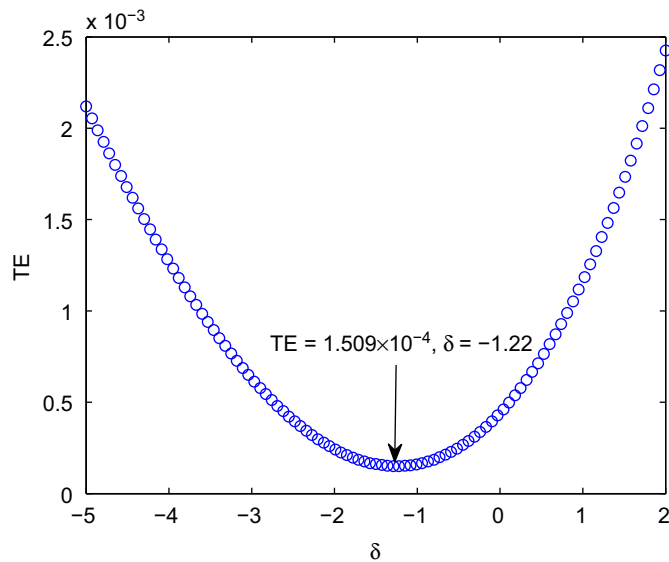


Fig. 13. The error curve of Example 3 with diagonal element $\hat{A}(i, i)$ ($N = 60$).

for this problem improves a little by searching the diagonal elements.

5. Conclusions

Numerical experiments have verified the present analytical diagonal elements of the RMM for the regular domain Dirichlet problems. We also find that the solution accuracy of the RMM is closely related to the diagonal elements of its interpolation matrix. Thus a searching process is employed to find the optimal diagonal elements for the RMM. As seen in the examples, the accuracies of the RMM solutions are improved with varying degrees for different domain problems. And an accurate subtracting and adding-back technique is essential to the RMM, which is a subject still under study.

Acknowledgments

The authors would like to thank the reviewers for their valuable suggestions to improve this paper. The work described

in this paper was partially supported by Natural Science Foundation of China (Project no. 10672051).

References

- [1] Belytschko T, Lu YY, Gu L. Element-free Galerkin methods. *Int J Numer Methods Eng* 1994;37:229–56.
- [2] Atluri SN, Zhu T. A new meshless local Petrov–Galerkin (MLPG) approach in computational mechanics. *Comput Mech* 1998;22:117–27.
- [3] Liu GR, Gu YT. A local radial point interpolation method (LRPIM) for free vibration analyses of 2-D solids. *J Sound Vib* 2001;246:29–46.
- [4] Hu HY, Li ZC, Cheng AHD. Radial basis collocation methods for elliptic boundary value problems. *Comput Math Appl* 2005;50:289–320.
- [5] Chen W, Hon YC. Numerical investigation on convergence of boundary knot method in the analysis of homogeneous Helmholtz, modified Helmholtz, and convection diffusion problems. *Comput Method Appl Mech* 2003;192:1859–75.
- [6] Chen JT, Chen IL, Chen KH, Yeh YT, Lee YT. A meshless method for free vibration analysis of circular and rectangular clamped plates using radial basis function. *Eng Anal Bound Elem* 2004;28:535–45.
- [7] Young DL, Chen KH, Lee CW. Novel meshless method for solving the potential problems with arbitrary domain. *J Comput Phys* 2005;209:290–321.
- [8] Golberg MA, Chen CS. The method of fundamental solutions for potential, Helmholtz and diffusion problems. In: *Boundary integral methods: numerical and mathematical aspects*. Boston, MA: WIT Press, Computational Mechanics Publications; 1999. p. 103–76.
- [9] Fairweather G, Karageorghis A. The method of fundamental solutions for elliptic boundary value problems. *Adv Comput Math* 1998;9:69–95.
- [10] Chen KH, Kao JH, Chen JT, Young DL, Lu MC. Regularized meshless method for multiply-connected-domain Laplace problems. *Eng Anal Bound Elem* 2006;30:882–96.
- [11] Young DL, Chen KH, Liu TY, Shen LH, Wu CS. Hypersingular meshless method for solving 3D potential problems with arbitrary domain. *Comp Model Eng Sci* 2009;40(3):225–69.
- [12] Chen KH, Kao JH, Chen JT, Wu KL. Desingularized meshless method for solving Laplace equation with over-specified boundary conditions using regularization techniques. *Comput Mech* 2009;43:827–37.
- [13] Young DL, Chen KH, Lee CW. Singular meshless method using double layer potentials for exterior acoustics. *J Acoust Soc Am* 2006;119:96–107.
- [14] Chen KH, Chen JT, Kao JH. Regularized meshless method for solving acoustic eigenproblem with multiply-connected domain. *Comput Model Eng Sci* 2006;16:27–40.
- [15] Chen KH, Chen JT, Kao JH. Regularized meshless method for antiplane shear problems with multiple inclusions. *Int J Numer Methods Eng* 2008;73:1251–73.
- [16] Chen JT, Chen PY. Null-field integral equations and their applications. In: *Boundary elements and other mesh reduction methods XXIX*. Southampton: WIT Press; 2007. p. 88–97.
- [17] Forsythe GE, Malcolm MA, Moler CB. *Computer methods for mathematical computations*. New Jersey: Prentice-Hall; 1977.
- [18] Song RC, Chen W. An investigation on the regularized meshless method for irregular domain problems. *Comput Model Eng Sci* 2009;42(1):59–70.